JCB

Article

Marching at the front and dragging behind: differential αVβ3-integrin turnover regulates focal adhesion behavior

Christoph Ballestrem, Boris Hinz, Beat A. Imhof, and Bernhard Wehrle-Haller

Department of Pathology, Centre Médical Universitaire, Geneva, Switzerland

Integrins are cell–substrate adhesion molecules that provide the essential link between the actin cytoskeleton and the extracellular matrix during cell migration. We have analyzed αVβ3-integrin dynamics in migrating cells using a green fluorescent protein–tagged β3-integrin chain. At the cell front, adhesion sites containing αVβ3-integrin remain stationary, whereas at the rear of the cell they slide inward. The integrin fluorescence intensity within these different focal adhesions, and hence the relative integrin density, is directly related to their mobility. Integrin density is as much as threefold higher in sliding compared with stationary focal adhesions. High intracellular tension under the control of RhoA induced the formation of high-density contacts. Low-density adhesion sites were induced by Rac1 and low intracellular tension. Photobleaching experiments demonstrated a slow turnover of β3-integrins in low-density contacts, which may account for their stationary nature. In contrast, the fast β3-integrin turnover observed in high-density contacts suggests that their apparent sliding may be caused by a polarized renewal of focal contacts. Therefore, differential acto-myosin–dependent integrin turnover and focal adhesion densities may explain the mechanical and behavioral differences between cell adhesion sites formed at the front, and those that move in the retracting rear of migrating cells.

Introduction

Modulation of cell–substrate adhesion plays a crucial role in cellular processes such as migration, spreading, or contraction. These morphological changes result from the coordinated reorganization of the actin cytoskeleton induced by intra- or extracellular stimuli (Lauffenburger and Horwitz, 1996). Cell migration is sustained by the continuous growth of actin filaments at the leading edge, and the controlled retraction of adhesive contacts at the rear of the cell (Palecek et al., 1998; Horwitz and Parsons, 1999; Ballestrem et al., 2000). Integrin αβ heterodimers provide the physical link between the continuously reorganizing actin cytoskeleton and components of the extracellular matrix (ECM)* during cell migration (Hynes, 1992). Different types of integrin-containing cell–substrate contacts have been described, of which focal complexes and contacts are the best studied. These two types of contacts have been distinguished according to several features including size, the site where they are formed in the cell, their age, their appearance in interference reflection microscopy, and their regulation by small GTPases (Geiger and Bershadsky, 2001). In fibroblasts, small point-like focal complexes form at sites of Rac1-dependent lamellipodia induction (Ridley et al., 1992; Nobes and Hall, 1995; Rottner et al., 1999), whereas large and elongated focal contacts localize to the ends of actin stress fibers upon RhoA activation (Ridley and Hall, 1992; Nobes and Hall, 1995; Amano et al., 1997; Rottner et al., 1999). The mechanical influence of acto-myosin–induced intracellular contractility and extracellular tension was suggested as a major factor converting focal complexes into focal contacts (Chrzanowska-Wodnicka and Burridge, 1996; Pelham and Wang, 1997; Riveline et al., 2001). In this study, we will use the general term focal adhesion, and will classify them according to their different behavior and localization in migrating cells as well as their integrin dynamics.

Although the pathways leading to the changes in the actin cytoskeleton are well understood, it is not known how the
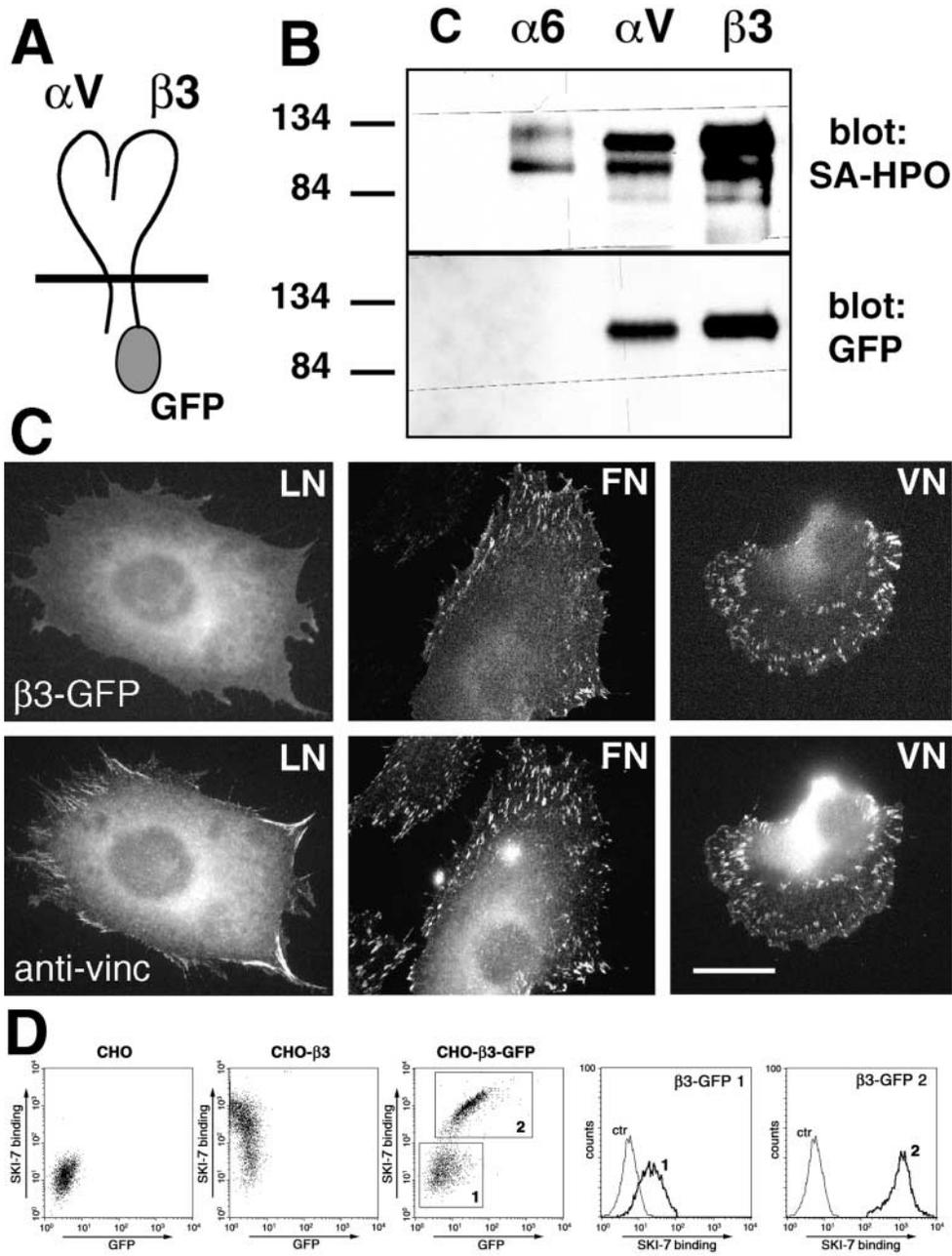
Figure 1. **The GFP-tagged β3-integrin chain forms functional heterodimers with endogenous αV.** (A) Scheme of the αVβ3–GFP-integrin heterodimer. The GFP protein is tagged COOH-terminally to the cytoplasmic domain of the β3 subunit. (B) Immunoprecipitations of cell extracts from surface biotinylated B16 β3–GFP cells. Extracts were precipitated with the indicated antibodies (c, control) and separated under reducing conditions by PAGE followed by transfer onto nitrocellulose membranes. Revelation with either streptavidin coupled horseradish peroxidase (SA-HPO, top) or anti-GFP antibodies (GFP, bottom) demonstrated the typical double-band pattern for integrin heterodimers and the coprecipitated GFP-tagged β3-integrin subunit, respectively. The position of the molecular mass markers is indicated to the left of the blots. (C) Substrate-specific clustering of the αVβ3–GFP-integrin into adhesions sites. B16 β3–GFP cells were plated overnight on glass coverslips, previously coated with 5 μg ml^{-1} laminin-1 (LN), 5 μg ml^{-1} fibronectin (FN), or 1 μg ml^{-1} vitronectin (VN). Cells were subsequently fixed and substrate adhesion sites were revealed by immunohistochemical detection of vinculin. Note that β3–GFP-integrin–positive adhesion sites were only found on fibronectin and vitronectin, which are ligands for αVβ3-integrin. In contrast, β3–GFP-integrin did not cluster on laminin-1, for which it is not a ligand. Because B16 cells use a different type of integrin receptor (α6β1) to adhere to LN than to FN or VN (α5β1, αVβ3), their morphology and migration behavior is different between these substrates (Ballestrem et al., 1998). (D) FACS analysis of nontransfected, β3-, and β3–GFP-transfected CHO cells with a Kistrin–CD31 fusion construct (SKI-7) (Legler et al., 2001). Note that the β3–GFP-transfected CHO clone is not homogeneous, exhibiting cells that lost β3-GFP expression, which reduces their SKI-7 reactivity to endogenous αVβ3-integrin levels (gate 1) (ctr; SKI-7, unpublished data). Bar, 20 μm.

strength of the integrin-mediated link between the actin cytoskeleton and the ECM is controlled to promote either firm adhesion or detachment. Nonaggregated integrins ex-

hibit a high lateral diffusion within the plasma membrane (Duband et al., 1988). However, upon extracellular ligand binding, integrins become anchored to the actin cytoskele-

ton by a large set of structural and regulatory proteins (Miyamoto et al., 1995), thereby forming cell–ECM adhesion sites. A "sliding" of β1-integrin–containing focal contacts has recently been demonstrated, and was suggested to represent weak attachment of stationary cells (Smilenov et al., 1999). In addition, the movement of α5β1-integrins on the ventral side of fibroblasts has been related to ECM reorganization by fibrillar adhesions (Katz et al., 2000; Pankov et al., 2000; Zamir et al., 2000).

To analyze the dynamics of individual integrin heterodimers within adhesion sites of migrating cells, we focused on the integrin αVβ3. Integrin αVβ3 is expressed on various motile cells such as neural crest cells (Delannet et al., 1994) and plays an important role in tumor metastasis (Albelda et al., 1990; Felding-Habermann et al., 2001), angiogenesis (Brooks et al., 1994), leukocyte transmigration (Weerasinghe et al., 1998), and osteoclast function (McHugh et al., 2000). Its ECM ligands include fibronectin, vitronectin, and fibrinogen (Cheresh and Spiro, 1987).

The use of a directly green fluorescent protein (GFP)-labeled β3-integrin chain that was coexpressed with the endogenous αV-integrin subunit on the cell surface allowed us to follow clustering and dispersal, and to perform quantitative analysis of αVβ3-integrins within adhesion sites of living cells. We specifically asked whether the organization of β3-integrins in focal adhesions differed according to their subcellular localization, and whether distinct organization patterns could be attributed to the activities of members of the Rho family of small GTPases. In particular, we studied the influence of intracellular tension, analyzed with the help of elastic silicon substrata, on the organization of β3-integrins within focal adhesion sites. Moreover, using FRAP, we analyzed the turnover rates of β3-integrins within different focal adhesions, in order to understand whether the motile behavior and function of a given focal adhesion site could be correlated to the temporal stability of the embedded integrins. We found differential densities of integrins within focal adhesion sites that correlated with the degree of actomyosin–dependent intracellular contraction, and an inverse correlation to the temporal stability of integrins within these sites. Our data reveal casual connections between the behavior of integrins and the state of the actin cytoskeleton that provides the base for a detailed mechanical model of cell migration.

Results

Dimerization of β3–GFP-integrin chain with αV

To study and quantify αVβ3-integrin dynamics in living cells, we generated a fusion protein of the β3 integrin subunit with GFP (Fig. 1 A). To determine whether this β3–GFP-integrin chain formed heterodimers with the endogenous αV subunit, we surface biotinylated stable β3–GFP-integrin–transfected cells (B16 F1 melanoma and 3T3 fibroblasts), and performed immunoprecipitations with antibodies against either the αV- or the β3-integrin subunits (Fig. 1 B). After precipitation of the integrin and subsequent Western blotting, both α- and β-integrin subunits could be detected with avidin-peroxidase (Fig. 1 B). Bands for the β3–GFP-integrin fusion protein were only detected in pre-

cipitations with anti–αV- or –β3-integrin subunits, but not with control rat serum nor with anti–α6-integrin subunit which forms heterodimers with the β1 and β4 chains (Fig. 1 B, bottom). These experiments clearly demonstrated that β3–GFP-integrin was expressed on the cell surface as a heterodimeric complex in association with the endogenous αV chain.

Ligand-specific clustering of αVβ3–GFP-integrin

To further test whether the αVβ3–GFP-integrin heterodimer was functional and did not unspecifically associate with cytoskeletal elements of focal adhesions, we plated β3–GFP-transfected cells on the αVβ3 ligands fibronectin and vitronectin, and on laminin-1, which is not a ligand for αVβ3. Clustering of GFP was observed on fibronectin and vitronectin, but not on laminin-1 (Fig. 1 C). Vinculin and paxillin are present in, and used as markers for, cell–substrate adhesion sites. Both localized to focal adhesion sites on all three substrates (Fig. 1 C, paxillin, unpublished data). In contrast, αVβ3-integrin–containing focal adhesions were only detected in cells cultured on fibronectin or vitronectin substrata (Fig. 1 C). To demonstrate that the transfected β3–GFP-integrin engaged in ECM binding was comparable to wild-type β3 chains, we analyzed stable β3–GFP- and β3-transfected CHO cells for their binding to a αVβ3-integrin–specific snake venom disintegrin (Kistrin). A FACS profile using a Kistrin–CD31 fusion protein (SKI-7) revealed only low levels of endogenous αVβ3-integrin in nontransfected CHO cells (Legler et al., 2001). In contrast, both β3- and β3–GFP-transfected cells displayed extensive SKI-7 reactivity (Fig. 1 D). These results demonstrate that αVβ3–GFP-integrin behaves like endogenous αVβ3, indicating that ligand binding, integrin signaling, and substrate specificity are not perturbed by the fusion of GFP to the β3-integrin chain. Moreover, these data suggest that the associated αV-integrin integrin chain specifically protects the cytoplasmic domain of β3–GFP from matrix-independent engagement with cytoskeletal elements of focal adhesions (Yauch et al., 1997). Therefore, direct labeling of the β3-integrin with GFP allowed us to follow and quantify β3-containing integrins in living cells.

Dynamics of β3-integrin

This αVβ3–GFP tool permitted now the direct observation of integrin clustering and turnover in adhesion sites of migrating or stationary cells. Therefore, we performed time-lapse experiments with stably β3–GFP-transfected, fast-migrating B16 F1 melanoma cells, or stationary 3T3 fibroblasts (B16 β3–GFP or 3T3 β3–GFP, respectively). In B16 β3–GFP cells, we observed the formation of small integrin clusters just behind the leading edge of the advancing lamellipodia (Fig. 2, A and B). These clusters remained stationary with respect to the substratum, whereas the cell moved forward. When GFP-containing focal adhesions reached a distance of 10 μm from the leading edge, they began to shrink and finally disappeared (Fig. 2, A, circled, and B, boxed; Video1, available at http://www.jcb.org/cgi/content/full/jcb.200107107/DC1). We noted that some of the focal adhesions in the smoothly protruding lamellipodia assumed an elongated shape. Although we never observed actin stress
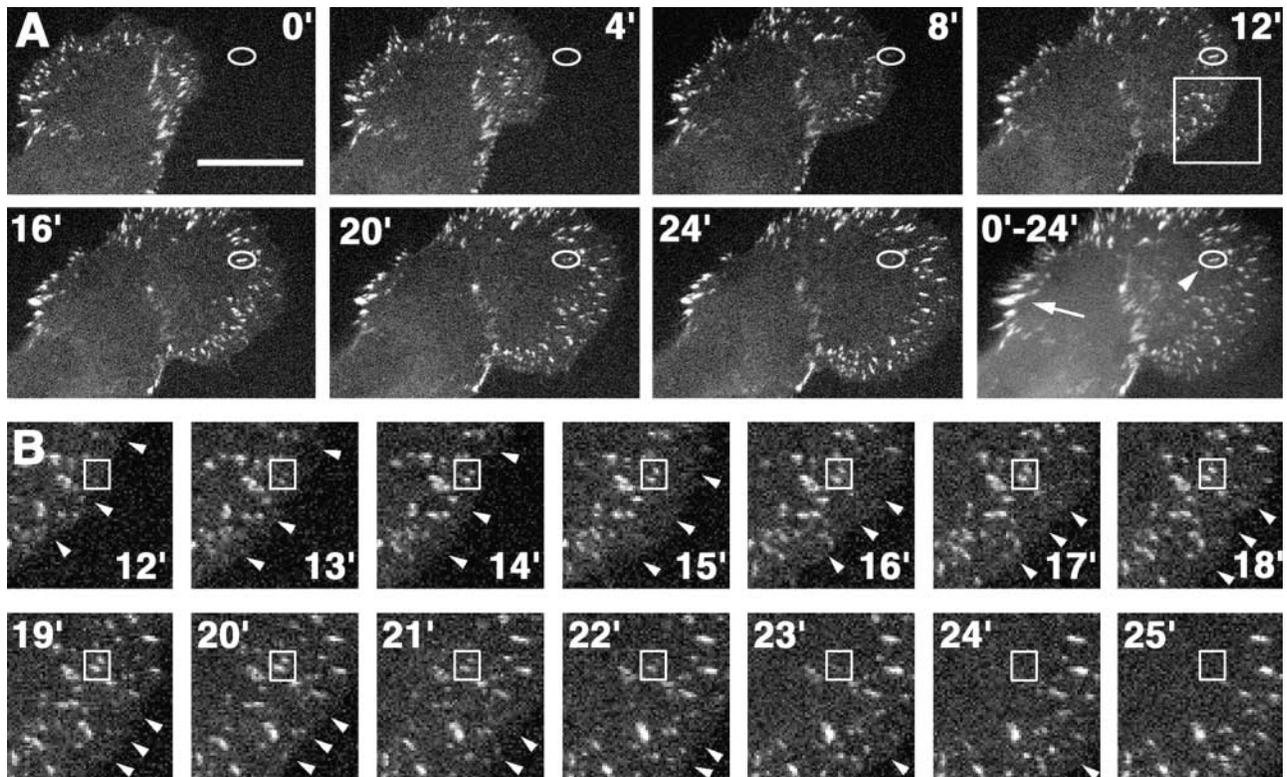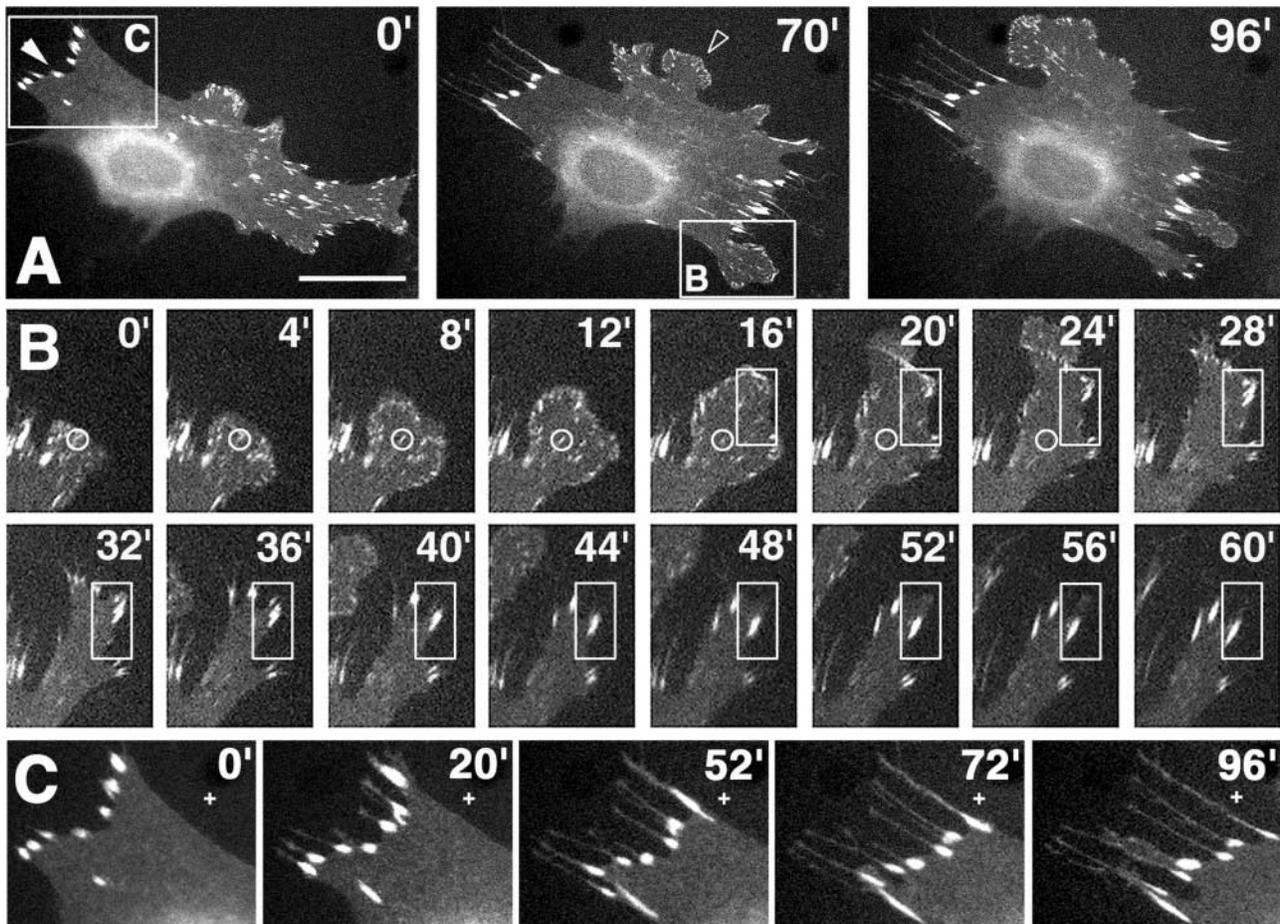
Figure 2. **Dynamics of β3–GFP-integrin in stable transfected B16 F1 cells.** Time-lapse analysis of a B16 β3–GFP cell plated overnight on vitronectin (1 μg ml⁻¹) revealed the transient β3–GFP-integrin clustering and subsequent dispersal in the advancing lamellipodium. A typical β3-integrin cluster (A, circled) appeared close to the leading edge (8′) and remained stationary (12′) until it began to gradually disappear (16′–24′). In retracting parts of the cells, integrin clusters began to slide inward (arrow). To appreciate the relative movement of the different integrin clusters during this time-lapse, an overlay revealed the stationary nature of focal adhesions in the lamellipodia (arrowhead) and the streak-like pattern of sliding focal adhesions in retracting parts of the cell (arrow). In B, a higher temporal and spatial resolution of the boxed area in A (12′) revealed the polymorphic appearance of the stationary integrin clusters (small box as reverence). Although shapes were variable, the fate of the clusters were identical. Arrowheads in B mark the smoothly advancing leading edge of the lamellipodium. Bar, 18 μm.

fibers in actively protruding lamellipodia, the presence of radially oriented actin ribs within the lamellipodia was frequent (Ballestrem et al., 1998). Continuous appearance and disappearance of stationary β3-integrin focal adhesions occurred within a restricted area in the advancing lamella. We refer to this area as the zone of transient integrin clustering. In posterior regions of the cell, integrin-containing focal adhesions moved in relation to the substratum during retraction (Fig. 2 A, arrow; Video2, available at http://www.jcb.org/cgi/content/full/jcb.200107107/DC1). To examine the possibility that integrin contacts in highly migratory melanoma cells might behave differently from stationary or slow moving fibroblasts (3T3 β3–GFP cells), we compared the appearance of GFP fluorescence in transfected B16 and 3T3 cells. 3T3 cells displayed continuous cycles of lamellipodia formation followed by retraction, and they showed comparable integrin cluster dynamics to what had been seen in B16 β3–GFP cells (Fig. 3; Video3, available at http://www.jcb.org/cgi/content/full/jcb.200107107/DC1). However, during collapse of lamellipodia, small focal adhesions in 3T3 cells transformed into larger, fluorescently brighter focal adhesions (Fig. 3 B). During retraction, these focal adhesions began to move in relation to the substratum (Fig. 3, B and C). In conclusion, our data show that αVβ3-integrins aggregate into stationary focal adhesions within the

zone of transient integrin clustering during the protrusion of lamellipodia. After the collapse of lamellipodia and subsequent retraction, small stationary focal adhesions transform into inwards sliding larger focal adhesions.

Induction of differential β3-integrin cluster densities upon transfection with dominant Rac1, Cdc42, and RhoA

Lamellipodia formation, as well as the retraction of cell edges, depends on the reorganization of the actin cytoskeleton. In addition, the transition from small and stationary to larger, retracting focal adhesions was associated with an increase in fluorescence intensity, and hence increased integrin density (Fig. 3). Because signaling through members of the Rho family of small GTPases is known to cause changes in the actin cytoskeleton (Ridley and Hall, 1992; Ridley et al., 1992; Nobes and Hall, 1995), we asked if changes in activation of these GTPases would influence the organization and density of αVβ3-integrin in focal adhesion sites. To answer this question, we transfected dominant active forms of Rac1, Cdc42, and RhoA into B16 β3–GFP cells, and quantified integrin fluorescence and focal adhesion morphology (Fig. 4). Control cells typically displayed a leading lamella with small β3-integrin– positive focal adhesions and larger, fluorescently brighter β3-integrin focal adhesions at the side and

Figure 3.   **Dynamics of β3–GFP-integrin in stable transfected 3T3 cells.** Time-lapse analysis of a 3T3 β3–GFP cell plated overnight on vitronectin (1 μg ml^{-1}), exhibiting cycles of lamellipodia extension (B) followed by cell edge retraction (B and C). During lamellipodia extension, transient stationary small focal adhesions formed behind the leading edge (B, circled focal adhesion). During cessation of the extension phase, small peripheral focal adhesions grew in size and were transformed into inward sliding focal adhesions (B, boxed area). Note that the start of the time lapse in B corresponds to 54′ in A. Continuous inward sliding of large focal adhesions occurred in parallel with cell edge retraction (C). A fiduciary mark on the substrate (C, white crosses) can be used to gauge the speed and position of retracting focal adhesions. Bar, 24 μm.

rear of the cell (Fig. 4 A). Expression of dominant active Cdc42 (V12) and Rac1 (L61) that are known to induce filopodia and lamellipodia, respectively (Ridley et al., 1992; Nobes and Hall, 1995), led to the appearance of flat and well-spread B16 β3–GFP cells. Compared with control cells the surface area increased by 188 and 248%, respectively (see Materials and methods), and cells exhibited actin-rich filopodia and lamellipodia and many small caliber actin filaments (unpublished data). This phenotype is apparent only after prolonged exposure to dominant active Rac1, and is associated with the formation of many small caliber actin filaments as previously reported (Ridley et al., 1992). In these cells, β3–GFP fluorescence resulted in a streak-like pattern of integrin clusters associated with filopodia (cdc42) or lamellipodia (Rac1) covering large areas of the substratum. These extensive clusters exhibited a granular pattern that resembled assemblies of numerous small focal adhesions (Fig. 4, B and C). The fluorescence intensity profiles indicated in Fig. 4, A–C, revealed that the density of β3-integrin in small focal adhesions in control cells (Fig. 4 E, profile a) corresponded to the densities measured across the integrin clus-

ters of dominant Cdc42- and Rac1-transfected cells (Fig. 4 E, profile da-Cdc42 and da-Rac1). In contrast, measurements of GFP intensity (and hence, integrin densities) in focal adhesions that were localized in retracting cell edges at the rear of control cells were consistently higher (Fig. 4 E, profile b). Moreover, expression of dominant active RhoA (V14) induced robust stress fiber formation and the cells appeared contracted (64% of control cell surface area) with large, even brighter fluorescent β3-integrin focal adhesions (Fig. 4, D and E, profile da-RhoA). From these data we calculated (see Materials and methods) that the relative αVβ3-integrin densities compared with nonclustered integrin in the plasma membrane increased by three- to fivefold in lamellipodial and Rac1- or Cdc42-induced low-density focal adhesions, by five- to eightfold in lateral and rear high-density focal adhesions of control cells, and by 9–14-fold in focal adhesions of dominant RhoA-stimulated cells (Fig. 4 F). Similar to the raise in integrin densities, we also observed a RhoA-dependent increase in anti-vinculin labeling of focal adhesions (unpublished data). These results demonstrate that the Rac1- and RhoA-induced changes in the bundling
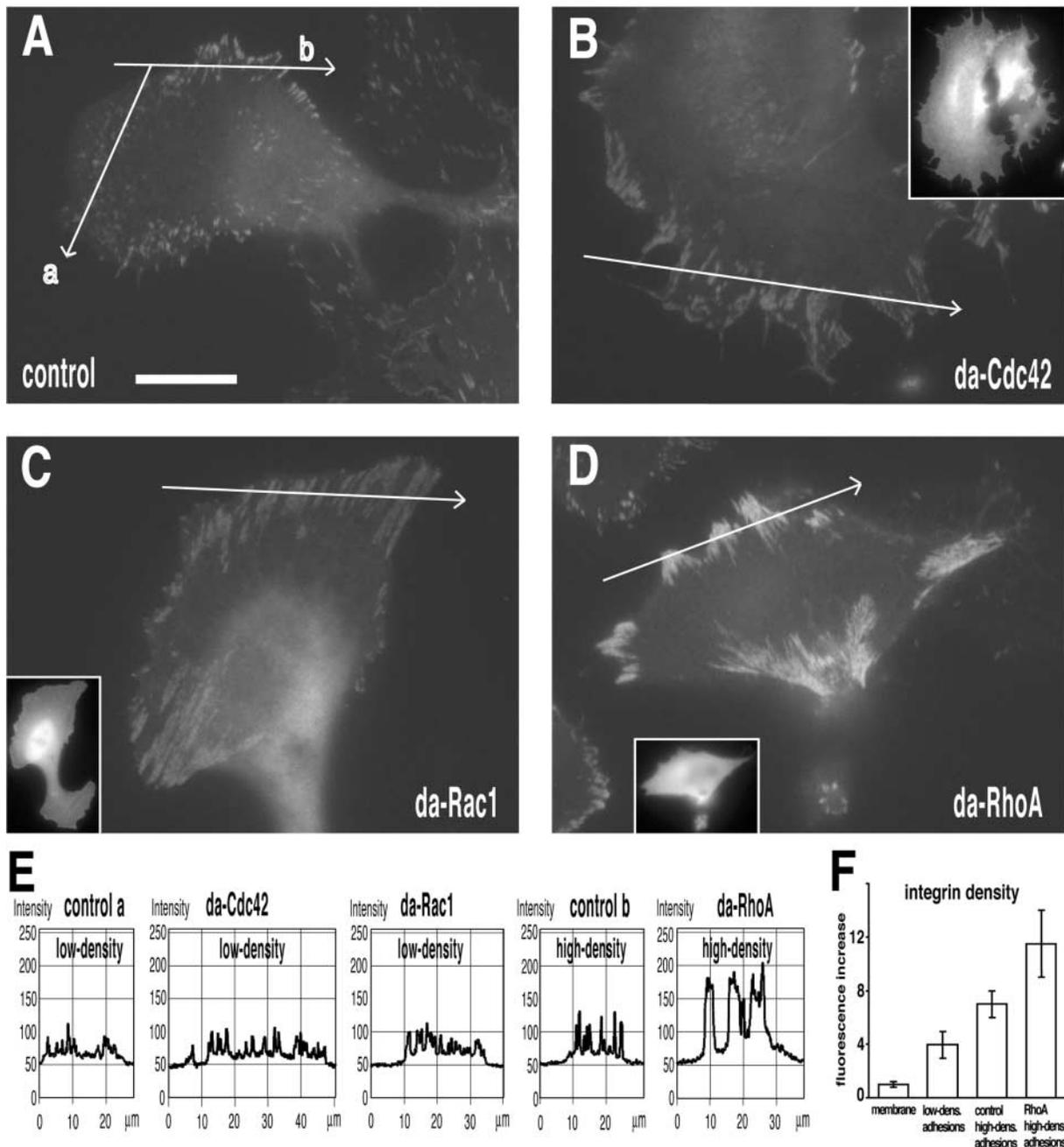
Figure 4.   **Members of the Rho family of small GTPases regulate β3-integrin clustering differentially.** B16 β3–GFP cells transfected with myc-epitope–tagged dominant active forms of Cdc42, Rac1, and RhoA were plated overnight on vitronectin (1 μg ml^{-1})-coated glass coverslips. Cells were fixed and stained for the expression of the myc-epitope (inserts), and GFP fluorescence images were recorded with identical camera settings in order to appreciate qualitative as well as quantitative differences in the integrin localization pattern. (A) Nontransfected control cells displayed the typical pattern of small low-fluorescent focal adhesions in the lamellipodium (profile a) and larger high-fluorescent focal adhesions at lateral borders and rear of the cell (profile b). (B) Dominant active Cdc42 (da-Cdc42) induced the formation of long, streak-like arrays of low-fluorescent β3 integrin focal adhesions mainly localized in the lamella or periphery of the cell. Similarly, dominant active Rac1 (da-Rac1) induced extensive β3-integrin clustering into low-fluorescent adhesion sites at the periphery of the cell (C). In contrast, dominant active RhoA (da-RhoA) induced a retracted cellular morphology with intensively fluorescent β3-integrin focal adhesions at the cell periphery (D). Fluorescence intensity profiles of the indicated traces in A–D are shown in E. Note that the intensity profiles are similar between focal adhesions in the lamellipodium of control cells and cells transfected with dominant active Cdc42 and Rac1. Peak fluorescent intensities of lateral and rear focal adhesions in control cells are consistently higher compared with lamellipodial focal adhesions, but can increase even more after dominant active RhoA induction. A quantification of the β3-integrin density (fluorescence intensity increase over membrane) is shown in F. Bar, 15 μm.

state of the actin filament network led to changes in the clustering behavior of β3 integrin, i.e., the generation of integrin low- and high-density focal adhesions, respectively.

Intracellular tension controls integrin density transition within focal adhesions

What causes this RhoA-induced increase in integrin density?
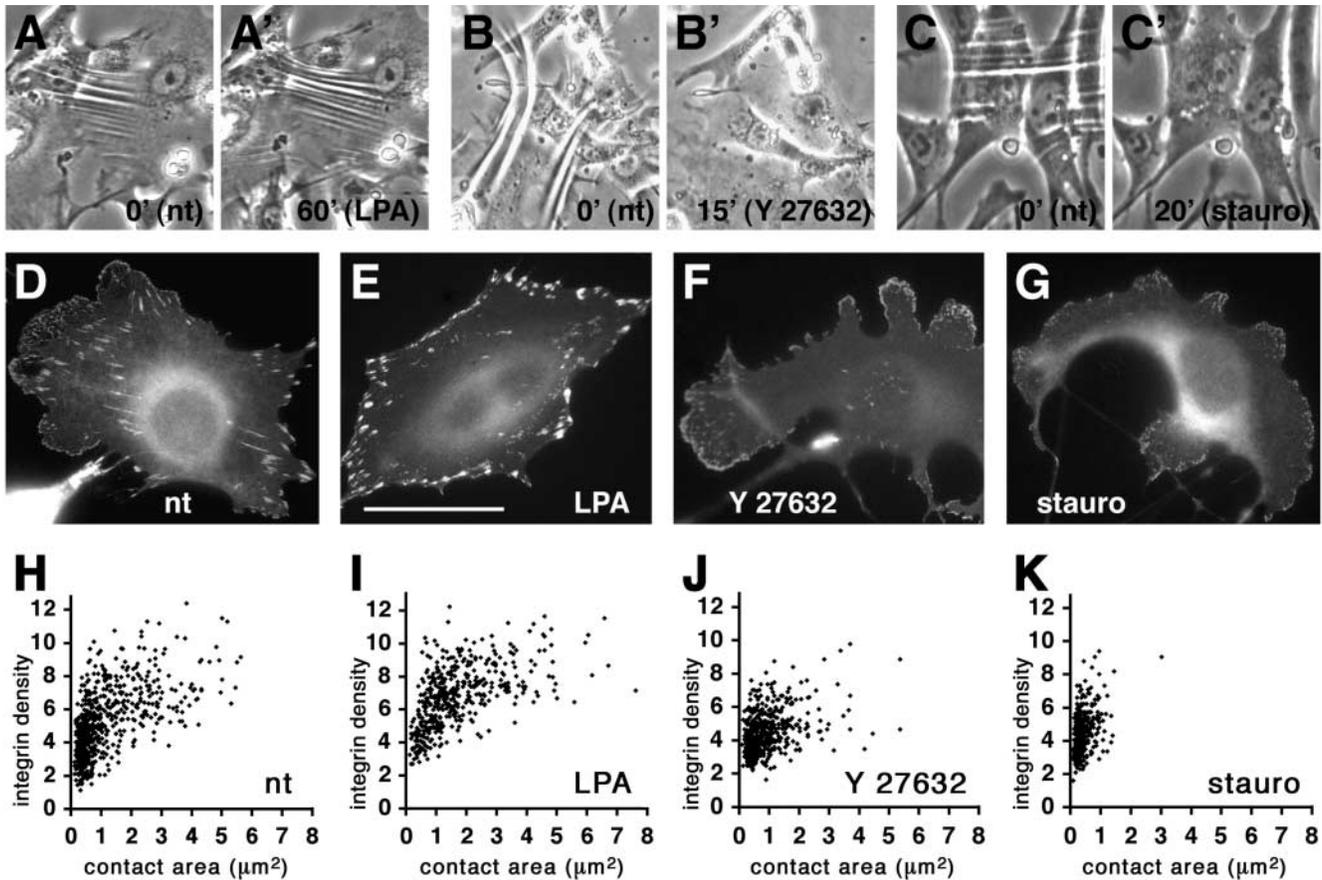
Figure 5. **Intracellular tension correlates with integrin density in focal adhesion sites.** 3T3 β3–GFP cells were grown on flexible silicone rubber substrates in order to visualize intracellular contractile forces by the appearance of substrate wrinkles. (A–C) Cells were recorded for 1 h under control conditions to confirm stability of the wrinkles (nt). After addition of drugs, the increase in substrate wrinkles (LPA, 10 μM) or their disappearance (Y 27632, 10 μM, or staurosporine, 50 nM) were recorded for the indicated times (A'–C') (Videos 4–6). In a parallel experiment, 3T3 β3–GFP cells were grown overnight on serum-coated glass coverslips (D, nt), and changes in β3–GFP-integrin localization in response to the above mentioned drugs was determined after 60 min of treatment (E, LPA; F, Y27632; G, staurosporine). The peak β3-integrin density/focal adhesion area relationship was plotted for untreated (H), LPA- (I), Y 27632- (J), and staurosporine- (K)treated cells. Note the shift in the focal adhesion population after addition of agonist. Bar: (A–C), 80 μm; (D–G), 40 μm.

Previously it has been shown that activated RhoA increases myosin-dependent contraction of the actin cytoskeleton, leading to intracellular tension (Chrzanowska-Wodnicka and Burridge, 1996; Amano et al., 1997). Integrins in focal adhesion sites are anchored within the actin cytoskeleton, such that contraction of this actin filament backbone induced by myosin activity may lead to increased integrin density, i.e., the transition of lamellipodial to lateral focal adhesions. To test this, we determined whether intracellular tension induced by RhoA was correlated with this transition. Intracellular tension was measured by plating 3T3 fibroblasts on flexible silicone rubber that formed wrinkles in response to cellular contraction (Harris et al., 1980). Activation of RhoA by lysophosphatidic acid (LPA) (10 μM) within these cells increased the number of wrinkles (Fig. 5 A; Video4, available at http://www.jcb.org/cgi/content/full/jcb.200107107/DC1) (Amano et al., 1997). RhoA activates Rho-kinase, which blocks myosin light chain phosphatase, resulting in myosin-dependent actin contraction (Kimura et al., 1996). Treatment of cells with the Rho-kinase inhibitor Y-27632 (10 μM) removed the wrinkles (Fig. 5 B; Video5, available at http://www.jcb.org/cgi/content/full/jcb.200107107/DC1)

(Uehata et al., 1997). Similarly, blocking of myosin light chain kinase with the wide-spectrum protein kinase inhibitor staurosporine (50 nM) resulted also in the disappearance of wrinkles (Fig. 5 C; Video6, available at http://www.jcb.org/cgi/content/full/jcb.200107107/DC1). Using these modulators of intracellular tension, the formation of high- and low-density focal adhesions was analyzed. Treatment of 3T3 fibroblasts with LPA increased β3-integrin compaction and formed high-density focal adhesions (Fig. 5 E). In contrast, cells treated with Y-27632 or staurosporine displayed the disappearance of high-density focal adhesions, whereas low-density focal adhesions remained in the periphery of the cells in the lamellipodia (Fig. 5, F and G). To correlate the changes in intracellular tension with that of the integrin density and focal adhesion size, we displayed the relative peak integrin density (compared with the integrin density in the membrane) and the respective area of focal adhesions (see Materials and methods). For each experimental condition, we analyzed ∼500 focal adhesions from different cells. Control cells displayed a significant number of small-sized, low-density focal adhesions that were mainly associated with protruding lamellipodia (Fig. 5 H). In addition, a considerable

Figure 6. **Block of intracellular tension reduces focal adhesion density.** Time-lapse analysis of β3-integrin fluorescence of focal adhesions in B16 β3–GFP cells after addition of Y-27632 (20 μM) (A, 5′ before addition; B, 60′ after addition). (C) Higher magnification of the boxed area in A demonstrates (a) the reduction in β3-integrin density (fluorescence intensity) during the first 10 min of treatment and (b) the further dispersal of compact β3-integrin focal adhesions into irregularly shaped β3- integrin clusters (arrowhead). (D) The average peak β3-integrin integrin density in the peripheral focal adhesions was measured before and after the addition of the inhibitor. The indicated time refers to the addition of inhibitor. Bar, 20 μm.
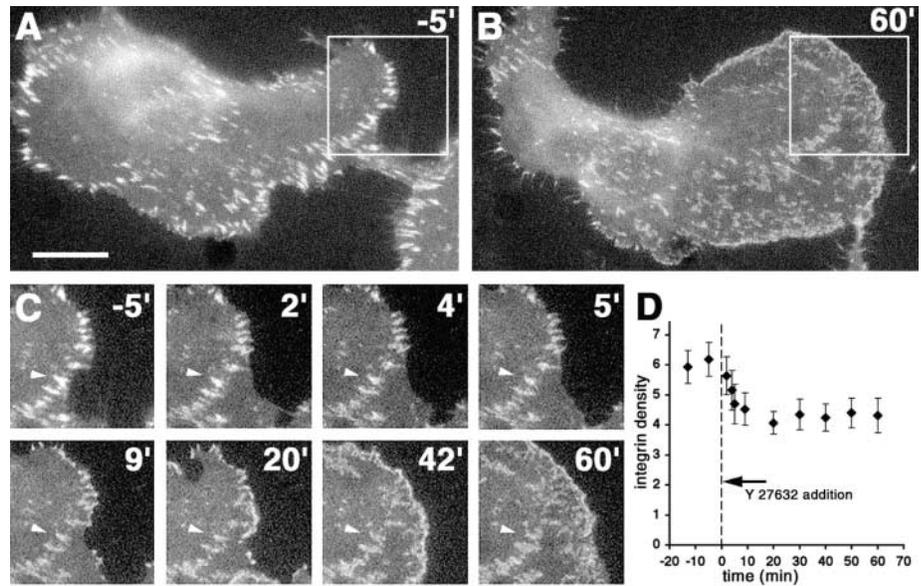
number of large-sized, generally high-density focal adhesions were found (Fig. 5 H) (average relative integrin density and size: 5.14-fold, 1.15 μm^2). The stimulation of the RhoA pathway with LPA led to a shift to denser and generally larger focal adhesions (Fig. 5 I) (average relative integrin density and size: 6.77-fold, 1.69 μm^2). In contrast, treatment with either Y-27632 or staurosporine resulted in a drop in integrin densities (Fig. 5, J and K). Interestingly, the average size of the contacts in Y-27632–treated cells was only slightly lower compared with control cells, whereas the average size of staurosporine treated contacts was dramatically reduced (average relative integrin density and size: Y-27632, 4.39-fold, 0.87 μm^2; staurosporine, 4.49-fold, 0.43 μm^2). Furthermore, the dynamic transition of high- to low-density focal adhesions was analyzed in living B16 F1 cells by time-lapse microscopy (Fig. 6; Video7, available at http://www.jcb.org/cgi/content/full/jcb.200107107/DC1). Release of intracellular tension by Y-27632 induced the rapid decrease in integrin densities in peripheral focal adhesions (Fig. 6, B and C, arrowhead). During the first 10 min of treatment, neither the shape of the contacts nor that of the cell did change. With time, the cell developed large lamellipodia that contained numerous dot-like tension-independent focal adhesions. In addition, the Y-27632–induced low-density focal adhesions began to change shape but remained undispersed during the entire time of observation (up to 90 min) (Video7, available at http://www.jcb.org/cgi/content/full/jcb.200107107/DC1). These observations suggest that high intracellular tension correlates with the formation and maintenance of high-density αVβ3-integrin focal adhesions. The formation of low-density αVβ3-integrin focal adhesions is favored under conditions of low intracellular tension.

Exchange rates of integrins differ between low- and high-density focal adhesions

In the previous experiments, we determined that the density of αVβ3-integrin and the apparent sliding of focal adhesions are critically linked to the tension created by the actin cytoskeleton in a Rac1/RhoA-dependent fashion. During cell migration, newly formed, small, stationary, low-density focal adhesions firmly anchor the cell to the substratum. At the cell rear, retraction and apparent sliding of high-density focal adhesions require a more flexible interaction with the substrate. To understand the mechanical differences between these two types of adhesion sites, it is necessary to determine the dynamics of integrins within these substrate contacts. Therefore, we performed FRAP of β3–GFP-integrins within high-density focal adhesions and compared it with the recovery of integrins in low-density focal adhesions. FRAP measurements of β3–GFP-integrins in high-density focal contacts revealed a fast exchange (Fig. 7 A). Within 120 s, 50% of the integrin fluorescence recovered in the bleached contacts, whereas the exchange of all the β3-integrins was completed within 5–10 min (mobile fraction [MF] = 80–100%) (Fig. 7 B). This exchange was independent whether a high-density focal adhesion was stationary or sliding (Fig. 7 A). Due to the transient nature of low-density focal adhesions within an advancing lamellipodia, it was impossible to measure FRAP (Fig. 2). Therefore, we analyzed low-density focal adhesions formed upon transfection with dominant active Rac1 (Fig. 4). These low-density focal adhesions revealed a 2.5× slower recovery of integrins than high-density focal adhesions (Fig. 7 B). In addition, during the time of observation recovery reached only 50% (MF), suggesting that half the integrins in low-density focal adhesions are immobilized. Our experiments showed that although the integrin density in Rac1-induced focal adhesions was lower (see above), the retention time of integrins was dramatically increased compared with high-density focal adhesions. These data also suggest that an increase in intracellular tension, and hence the activation of RhoA, increases the turnover rate of integrins in focal adhesions.

Discussion

Migration is a complex cellular behavior that involves protrusion and adhesion at the cell front, and contraction and detachment at the rear. During these processes, members
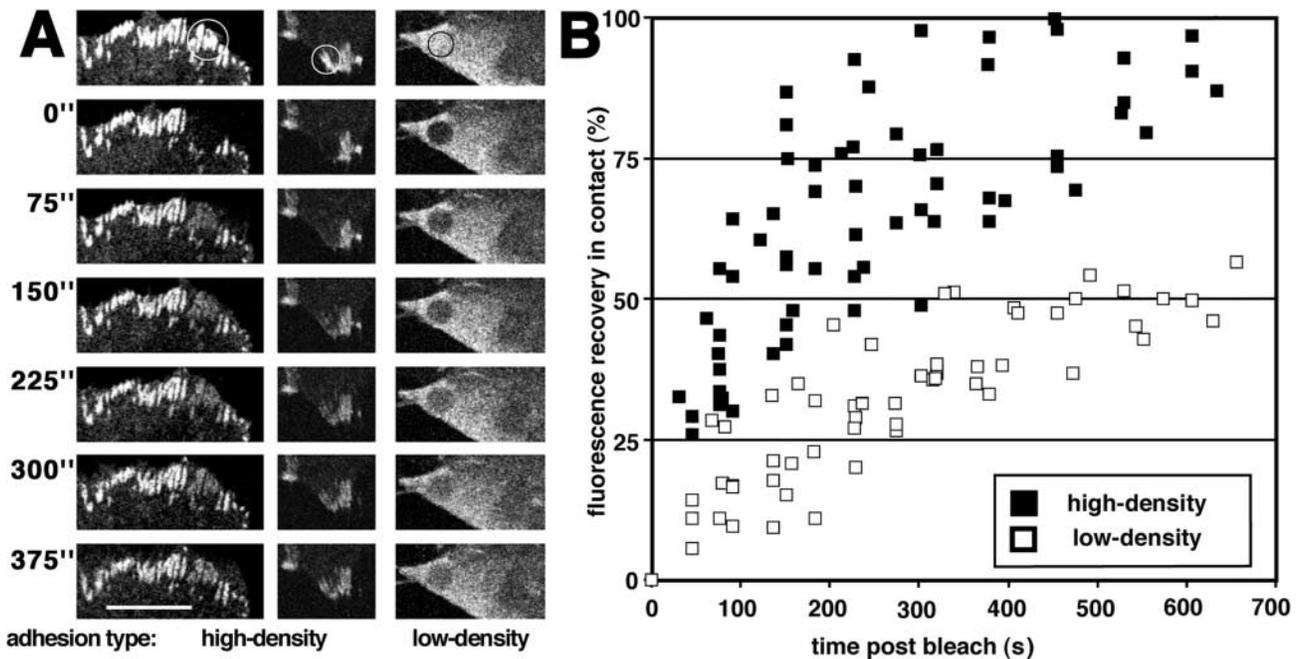
Figure 7.   **FRAP reveals different β3-integrin exchange rates in high- versus low-density focal adhesions.** (A) Nontransfected or dominant active Rac1 transfected B16 β3–GFP cells were cultured overnight on serum-coated glass coverslips and FRAP was performed on focal adhesions localized to the edge of cells. The bleached area of each series is circled in the first frame and the recovery time (seconds after completion of bleach) indicated to the left. In control cells, immobile (first series) and inward sliding (second series) high-density focal adhesions show almost complete recovery (MF >80%). In cells transfected with dominant active Rac1 (third series) in which low-density focal adhesions were formed, fluorescence recovery was only partial (50% MF), reaching fluorescent levels just slightly above fluorescence intensities of nonclustered β3–GFP-integrin present in the plasma membrane (visible on the right hand side of the frame). Qualitative FRAP curves from several cells (5–8) are displayed in B. Each data point is the median of three to five individual focal adhesions. Bar, 10 μm.

of the integrin family provide the physical link between the actin cytoskeleton and the extracellular environment (Hynes, 1992). Here, we developed a new tool to follow and quantify αVβ3-integrins within focal adhesions formed in living cells by GFP labeling of the β3-integrin subunit (Plancon et al., 2001) for a similar construct). We have chosen the β3-integrin subunit for GFP tagging, as it forms heterodimers uniquely with the V and the platelet-specific IIb α chains. Therefore, GFP–β3-integrin transfected into cells (except platelets), will pair exclusively with αV to create a single species of labeled integrins. Most importantly, for quantitative studies of integrins, the amount of GFP fluorescence correlates directly with the number of αVβ3 heterodimers, and represents a direct measure of the relative integrin density within the two-dimensional plasma membrane and focal adhesion sites. In addition, the β3–GFP-integrin subunit, like normal β-integrin chains, requires heterodimerization with the αV chain for ER export and for an ECM-dependent engagement into focal adhesions (Heino et al., 1989; Lenter and Vestweber, 1994; Yauch et al., 1997). This is in contrast to monomeric chimeric β-integrin constructs that associate with focal adhesions in an ECM-independent manner, and therefore are not suited for quantitative measurements of integrin behavior (LaFlamme et al., 1994; Smilenov et al., 1999). Our analysis of αVβ3-integrin–containing contacts in migrating and stationary cells revealed two differently behaving types of cell adhesion sites. At the cell front, stationary focal adhesions formed within a zone of transient

integrin clustering, whereas focal adhesions in retracting cell processes moved in relation to the substratum. The relative abundance of these two types of contacts may determine the migratory behavior of a cell. In the short-lived lamellipodia of slow-migrating fibroblasts, the zone of transient integrin clustering was difficult to define. In contrast, extremely fast-moving cells such as fish keratocytes exhibit stationary focal adhesions throughout the entire width of the lamellipodium that represent a major part of their total cell area (Lee and Jacobson, 1997; Anderson and Cross, 2000). Thus, the size of the area occupied by stationary focal adhesions, in respect to the total cell area, may determine the stability and persistence of lamellipodial protrusion and hence the overall speed of cell locomotion. In these different cell types, the zone of transient integrin clustering is equivalent to the area that is occupied by actin filaments originating at the edge of the lamellipodium (Svitkina et al., 1997; Ballestrem et al., 1998). It is conceivable that the actin filament turnover within the lamellipodium determines the half-lives of these stationary focal adhesions. In contrast to the stationary focal adhesions at the front of migrating cells, focal adhesions in retracting cell edges move relative to the substratum. This mobility of focal adhesions, previously described as sliding, has been suggested important for cell edge retraction and migration (Smilenov et al., 1999; Anderson and Cross, 2000; Zamir et al., 2000). Because the efficiency of cell migration is determined by the speed and ability of rear retraction (Palecek et al., 1998; Ballestrem et al., 2000), the

degree of focal adhesion sliding may limit the maximal speed of cell migration.

The quantitative analysis of GFP-labeled αVβ3-integrin allowed us to determine the changes in integrin densities within different types of focal adhesions. Hence, we observed a low αVβ3-integrin density in small, stationary focal adhesions, and a high αVβ3-integrin density in large, sliding focal adhesions. The formation of small dot-like focal adhesions (named focal complexes) in response to Rac1 and Cdc42 activation was first described by Nobes and Hall (1995) in fibroblasts, and they were distinguished from larger RhoA induced focal adhesions (named focal contacts) by their size (Nobes and Hall, 1995; Rottner et al., 1999). It is likely that these focal complexes and focal contacts are homologous to the low-density, respectively high-density focal adhesions observed by us. However, in contrast to focal adhesion size, integrin density represents a parameter that enables one to distinguish focal complexes from focal contacts in many different cell types, where the size differences are less accentuated as in fibroblasts, and is more specific than the recently questioned interference reflection microscopy (Iwanaga et al., 2001). Because activation of RhoA induces the bundling of actin filaments into stress fibers (Chrzanowska-Wodnicka and Burridge, 1996; Machesky and Hall, 1997), we suggest that the acto-myosin–dependent contraction of the actin scaffold increases integrin density in focal adhesions. This idea is supported by the observation that the gradual raise in acto-myosin–dependent intracellular tension strictly correlates with the amount of stress fiber formation and the increase in size of focal adhesions (Balaban et al., 2001). The increase in focal adhesion size has been recently attributed to RhoA activated mDia1, resulting in de novo actin polymerization at sites of focal complexes (Riveline et al., 2001). In contrast to RhoA, Rac1 or Cdc42 induces the formation of a looser actin filament lattice (Machesky and Hall, 1997) that could form the initial scaffold for low-density focal adhesions. The fate of these low-density focal adhesions, and hence their respective size and density, is then independently controlled by mDia1-stimulated actin polymerization and RhoA/Rac1-regulated acto-myosin contraction, respectively (Ridley et al., 1992; Sanders et al., 1999; van Leeuwen et al., 1999; Riveline et al., 2001). The importance of mechanical tension for focal adhesion compaction was corroborated by studies analyzing fields of intracellular tension during cell migration (Dembo and Wang, 1999; Oliver et al., 1999). In the lamellipodia of fish keratocytes, tension was low and isometric, predicting stationary low-density focal adhesions, whereas tension was high and vectorial at the lateral edges of the cell consistent with the formation of sliding high-density focal adhesions (Oliver et al., 1999; Anderson and Cross, 2000).

We have concluded that the integrin density within focal adhesion sites is determined by the degree of intracellular tension. Accordingly, changes in the elasticity of the ECM must similarly influence integrin density. We propose the following model. During cell migration, newly formed adhesion sites at the cell front are always in a low-density configuration. Subsequently, these sites mature into high-density contacts upon acto-myosin–dependent contraction. A rigid substratum such as glass resists the intracellular contraction resulting in a distortion of the actin integrin linkage. This mechanical stress within the focal adhesion site generates a signal for actin polymerization and growth of the focal adhesion. In contrast, an elastic ECM substratum will not resist the acto-myosin–dependent focal adhesion contraction failing to generate a distortion signal that would enforce the focal adhesion. Therefore, cells will favor a rigid over an elastic substrate for adhesion, a behavior consistent with the observed increase in cell motility and reduced spreading of fibroblasts on elastic substrates (Pelham and Wang, 1997). Furthermore, we propose that integrin density within a focal adhesion may act as a relay to exchange information about the degree of intracellular tension and extracellular elasticity, hence allowing cells to respond to gradients of extracellular elasticity and to adapt to mechanical distortions of the extracellular environment (Lo et al., 2000; Jalali et al., 2001; Riveline et al., 2001).

Induction of intracellular tension leads to the apparent sliding of focal adhesions in the rear of the cells. What is the mechanism of contacts sliding and how is αVβ3-integrin involved in this process? Focal adhesion have been considered as stable anchor points of the cell, supported by the observation that integrin containing fragments are left on the tracks of migrating cells (Chen, 1981). However, more recently it has become clear that fast-migrating cells recover integrins from the retracting, trailing portion of their body (Palecek et al., 1998; Pierini et al., 2000). Our FRAP analysis demonstrated a complete exchange of αVβ3-integrins in high-density focal adhesions within 5–10 min. This fast integrin turnover may provide a mechanistic explanation for focal adhesion sliding, resulting from a polarized renewal of integrins. We propose that the continuous loss of integrins from the distal edge, and recruitment of new integrins at the proximal edge of focal contacts, creates the illusion of sliding. In addition, high integrin turnover would increase the plasticity of focal adhesions, permitting rapid responses to local changes in intra- or extracellular tension. Because integrin turnover requires the loss of intracellular as well as extracellular links, the apparent turnover rates of integrins depend on the respective rate-limiting binding reaction. Measurement of fibrinogen to αIIb/β3 integrin affinity revealed a dissociation constant in the mM range (Rivas et al., 1996). Due to this low binding affinity, the rate-limiting step for integrin turnover is likely to be determined by the interaction of the integrin with the actin cytoskeleton.

Focal adhesions that are formed at sites of Rac1 activity at the cell front exhibit a surprisingly slow turnover and high temporal stability. Recently, it has been reported that Rac1 activation induces the high-affinity state of αVβ3-integrins, preferentially located within the leading edge of the cell (Kiosses et al., 2001). We propose that the slow and fast turnover rates of αVβ3-integrin in different focal adhesions directly represent its respective high- and low-affinity state. Hence, the high-affinity state of αVβ3-integrin in low-density focal adhesions may result in their stationary nature, whereas the low-affinity state in high-density focal adhesions may lead to their sliding. The RhoA signaling pathway leads to accumulation of phosphorylated myosin light chains, which in turn results in focal adhesions exhibiting high αVβ3-integrin turnover rates. Activation of the RAS/MAPK/
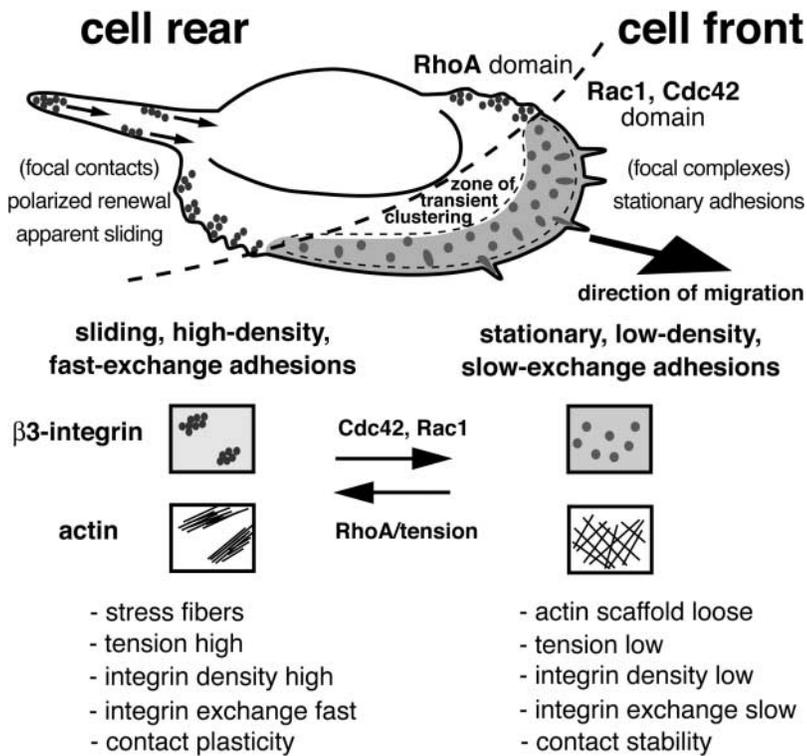
Figure 8. **Model of cell migration based on differential integrin turnover.** Cell migration is driven by Rac1- and Cdc42-dependent actin polymerization in the advancing lamellipodium. Integrin αVβ3 is incorporated in the lamellipodial actin filament lattice (gray shading) to form low-density integrin focal adhesions (focal complexes) (large and irregular shaped dots). These low-density focal adhesions remain stationary in respect to the substrate, firmly anchored in the cytoskeletal scaffold due to their slow turnover rate. These stabilized focal adhesions support the advancing lamellipodium. At the rear of the zone of transient clustering (circumferenced by dotted line), stationary focal adhesions rapidly disperse due to the depolymerization of the lamellipodial actin filament lattice (gray shading). While the cell moves forward, low-density focal adhesions at the lateral edges of the lamellipodium transform into high-density integrin focal adhesions (focal contacts) (accumulation of small dots). This transformation is directed by the acto-myosin–driven local collapse of the lamellipodial actin filaments into stress fibers and provides a means to sense the rigidity of the substrate. Integrins localized in high-density focal adhesions loose their firm cytoskeletal anchor and begin to show fast turnover, creating a great degree of plasticity for modulation of the contact. This plasticity can lead to polarized renewal of focal adhesions, the loss of integrins from the distal edge and their addition at the proximal edge of the contact, giving the illusion of sliding (small arrows).

ERK signaling pathway also results in myosin light chain phosphorylation. This pathway induces the low-affinity states of integrins and enhances rear retraction (Hughes et al., 1997; Klemke et al., 1997; Nobes and Hall, 1999; Fincham et al., 2000). These data suggest that myosin light chain phosphorylation might be the key step to the generation of low-affinity integrins in high-density focal adhesions that results in fast integrin turnover and is required to generate the sliding phenotype of these focal adhesions. Consistent with this hypothesis, it has recently been demonstrated that the RhoA signaling pathway, involving Rho-kinase and acto-myosin contraction, is required for integrin recycling and tail retracting of migrating leukocytes (Niggli, 1999; Pierini et al., 2000; Worthylake et al., 2001). Moreover, it has been demonstrated that nascent focal adhesions at the front of migrating fibroblasts generate the strongest propulsive forces (Beningo et al., 2001). These contacts display the typical phenotype of low-density and slow-turnover integrin contacts defined by this study.

To conclude, we propose a model of dynamic integrin clustering and dispersal in motile cells (Fig. 8). Rac1 and Cdc42 become activated and induce filopodia and lamellipoda that exhibit many stationary, low-density focal adhesions. Maximal cell motility is maintained by their ability to form firm adhesions due to slow integrin turnover and rapid dispersal at the rear of the zone of "transient integrin clustering," possibly caused by the depolymerization of lamellipodial actin filaments. Low-density focal adhesions form independent of intracellular tension, but transform into integrin dense focal adhesions at the lateral edge of the lamellipodium in response to RhoA induced acto-myosin–dependent intracellular tension. During this contraction, the actin inte-

grin linkage senses the mechanical condition of the contacted ECM substrate resulting in the enforcement of focal adhesions on rigid substrates. High-density focal adhesions maintained by high traction forces at the lateral borders, begin to slide and subsequently detach due to their fast integrin turnover, a prerequisite for cell migration. Therefore, acto-myosin induced integrin turnover would offer a crucial therapeutic target to control migratory behavior of many cell types and might be relevant for pathological situations involving excessive migration of cells.

Materials and methods

β3–GFP-integrin fusion protein
Full-length mouse β3-integrin cDNA was provided by Dr. Patrick Ross (Washington University School of Medicine, St. Louis, MO) (Weerasinghe et al., 1998; Legler et al., 2001). Fusion of the enhanced GFP (EGFP) coding sequence (CLONTECH Laboratories, Inc.) with β3-integrin cDNA was performed in two steps. First, a COOH-terminal fragment of β3-integrin, containing a unique EcoRV site (underlined), was amplified with a 5′-ATG-GATCCAAGGGTCCTGATATCCTG-3′ forward and 5′-AATACCGGTGA-AGTCCCCCGGTAGGTGATA-3′ reverse primer pair, in order to remove the stop codon. The amplified sequence was digested with BamHI (5′) and AgeI (3′) restriction enzymes and cloned into pcDNA3/EGFP, containing the EGFP cDNA sequence 3′ to an AgeI site. pcDNA3/EGFP was prepared by insertion of the HindIII/NotI EGFP containing fragment from pEGFP-N1 (CLONTECH Laboratories, Inc.) into pcDNA3 at these sites (Invitrogen). The remaining NH2-terminal part of the β3-integrin cDNA sequence (5′ to the EcoRV site) was cut out of the original vector with BamHI and EcoRV, and inserted at the respective sites into pcDNA3/EGFP, resulting in full-length β3–GFP-integrin joined by a short spacer (SerProValAlaThr).

Cells and transfections
NIH 3T3 fibroblasts and mouse B16F1 melanoma cells were cultured in DME and CHO cells in F12 medium, both supplemented with antibiotics and 10% FCS as described (Ballestrem et al., 1998). Superfect (QIAGEN)

or Fugen 6 (Roche) were used according to the manufacturers' recommendation for stable and transient transfections. Cells were cultured in the presence of 1 mg ml^{-1} G418 (GIBCO BRL) to select for stable β3–GFP-integrin–expressing clones (B16 β3–GFP; 3T3 β3–GFP).

NH$_2$ terminally myc-tagged (9E-10 epitope) (Evans et al., 1985) cDNA's for dominant active (L61) Rac, dominant active (V12) Cdc42, and dominant active (V14) RhoA, all in pRK5, were provided by Dr. Kurt Ballmer-Hofer (Paul Scherrer Institute, Villigen, Switzerland). The DS Red expression vector was obtained from CLONTECH Laboratories, Inc.

Antibodies and immunofluorescence

Anti–human vinculin were obtained from Sigma-Aldrich (Cat # V-9131). Mouse anti–chicken paxillin (clone 349) was from Transduction Laboratories, and mouse anti–myc (9E-10) was from American Type Culture Collection. The Kistrin–CD31 fusion protein (SKI-7) and the rat anti-CD31 monoclonal antibody (CG51) were used for FACS analysis as described (Legler et al., 2001).

B16 β3–GFP and 3T3 β3–GFP cells were cultured overnight in complete culture medium on Lab-Tek chambers (Nunc), previously coated with 5 μg ml^{-1} laminin-1, a gift from M. Chiquet (Morris Mueller Institute, Bern, Switzerland), 5 μg ml^{-1} fibronectin (Biomedical Products), or vitronectin 1 μg ml^{-1} (Sigma-Aldrich). Cells were fixed for 10 min with 4% paraformaldehyde in PBS and permeabilized with 0.5% Triton X-100 in PBS, washed, and blocked with PBS supplemented with 1% BSA. Cells were incubated 1 h with the respective monoclonal antibody diluted in PBS supplemented with 1% BSA. After rinsing twice with PBS, cells were incubated in the presence of goat anti–mouse antibodies conjugated to Texas red diluted in PBS supplemented with 1% BSA (Jackson Laboratories Inc.) and washed three times with PBS. Stained cells were examined and photographed using a Zeiss Axiovert 100 TV microscope equipped with a digital CCD camera (Hamamatsu Photonics) controlled by the Openlab software (Improvisions).

Immunoprecipitations

B16 β3–GFP were harvested by trypsinization and washed twice in ice-cold PBS before surface biotinylation with 0.5 mg ml^{-1} sulfo NHS-biotin (Pierce Chemical Co.) in PBS. Biotinylation was stopped by washing the cells in 2 ml ice-cold FCS. After three more washes in ice-cold PBS, cells were lysed in extraction buffer (1% Triton X-100, 0.5% deoxycholate, 0.1% SDS, 120 mM NaCl, and protease inhibitors) for 20 min at 4°C. Cell lysates were centrifuged at maximal speed for 15 min in a precooled microfuge. Supernatants were precleared with protein G beads (Amersham Pharmacia Biotech), and subsequently incubated overnight at 4°C with rat serum as control, a rat monoclonal against the integrin α6 subunit (EA-1) (Ruiz et al., 1993), a rat monoclonal against the αV subunit (RMV-7) (Takahashi et al., 1990), and a hamster anti-β3 subunit (anti-αVβ3, Cat # 01522D; PharMingen), coupled to protein G beads. Beads were washed four times in extraction buffer and then boiled in SDS sample buffer. An equivalent of 10^6 cells per lane was run under reducing conditions on 7% SDS PAGE gel. Proteins were transferred to nitrocellulose membranes and nonspecific binding sites were blocked with TBS containing 1% BSA and 0.1% Tween-20. After incubation with streptavidin–horse radish peroxidase or polyclonal rabbit anti-GFP antibodies (CLONTECH Laboratories, Inc.) followed by peroxidase-conjugated anti–rabbit immunglobulin antibodies (Sigma-Aldrich), peroxidase activity was visualized by chemiluminescence (ECL; Amersham).

Flexible silicone rubber contraction assay

Flexible rubber silicone substrata were prepared as described previously (Harris et al., 1980) with some modifications in order to obtain even and thin substrata. 5 μl of silicone fluid (poly dimethyl siloxane; 30,000 centistokes; Dow Corning) were deposited onto glass coverslips and centrifuged at 1,000 rpm for 1 min. The silicone surface was then crosslinked by passing the coverslip through a very low Bunsen flame for ~0.5 s. An incubation chamber was created by placing a silicone ring onto the coverslip. Silicone substrates were equilibrated with 0.1% gelatin in Tris-HCl buffer, pH 8.4 to facilitate cell adhesion, sterilized by UV light exposure for 3 h and left overnight in the incubator at 37°C. 3T3 fibroblasts were then seeded in DME/10%FCS and allowed to spread and to deform the silicone substratum for 2 d. Live cells were observed at 37°C on a Zeiss Axiovert microscope using a 32× Ph2 objective. Cells were recorded (KS400, 1 frame/15 s) for 60 min under control conditions before agonists were added to the culture medium. Three experiments were performed per experimental condition.

Time-lapse and inhibitor studies

Time-lapse studies were performed as described (Ballestrem et al., 1998, 2000). Briefly, B16 β3–GFP and 3T3 β3–GFP were cultured overnight on

Lab-Tek chambers previously coated overnight at 4°C with indicated concentrations of ECM proteins. Cells were visualized on an Axiovert 100 TV inverted microscope (Zeiss), equipped with an incubation chamber, a standard GFP filter set (Omega), and a Hamamatsu C4742–95–10 digital charge coupled device camera. Images were recorded in intervals of 1 or 2 min and processed using Openlab software (Improvision).

LPA and staurosporine were obtained from Sigma-Aldrich and used at 10 μM and 50 nM, respectively. Rho kinase inhibitor Y-27632 (Uehata et al., 1997) was obtained from Yoshitomi Pharmaceutical Industries and used at 10 μM for 3T3 β3–GFP cells, and at 20 μM for B16 β3–GFP cells.

Measurement of fluorescence intensities of integrin clusters and cell surface areas

Stable and homogeneously β3-integrin–expressing B16 β3–GFP and 3T3 β3–GFP cells derived from clonal selection were either transiently transfected with dominant active Rac1, Cdc42, and RhoA or treated with various drugs (see above). 24 h after transfection, or 1 h after the addition of drugs, cells were fixed and, where appropriate, were counterstained with anti-myc (9E-10) anti–mouse Texas red, in order to detect the transfected GTPases. GFP fluorescence images were recorded with identical exposure settings for all different experimental conditions on an Axiovert 100TV equipped with a CCD-camera (see above). Cell surface and focal adhesion areas and their respective mean and peak fluorescence were measured using the Openlab software (Improvision). For the GTPase transfection experiments, 20 or more cells were measured per experimental condition, and mean surface areas were calculated (nontransfected, 1127 ± 283 μm^2; da-Rac1, 2800 ± 1072 μm^2; da-Cdc42, 2117 ± 500 μm^2; da-RhoA, 724 ± 315 μm^2; data from one out of three qualitatively similar experiments). Fluorescence intensity profiles were obtained with the software of the LSM510 confocal microscope (Zeiss). The range of fluorescence values (expressed in 8-bit gray levels) were derived from several intensity profiles (three to five profiles per cell, from three to five different cells per condition) by determining the local minima and maxima: 48–52 (background fluorescence outside of cells), 65–75 (nonclustered integrin fluorescence in the cell periphery corresponding to two sheets of plasma membrane), 90–110 (peak fluorescence intensities of focal complexes in control, da-Rac1-, or da-Cdc42-transfected cells), 110–140 (peak fluorescence intensities of focal contacts in control cells) and 150–200 (peak fluorescence intensities of focal contacts in RhoA transfected cells). To calculate the relative increase in integrin densities in respect to the density of nonclustered integrins in one sheet of plasma membrane, we subtracted the background fluorescence (50) and the fluorescence of one of the plasma membrane sheets (10) from each value and divided it by the fluorescence of one plasma membrane sheet (10).

The same type of calculation was used to determine the x-fold fluorescence increase between the relative integrin density of membranes and that of individual focal adhesions in normal and drug treated cells. To develop an integrin density/contact area profile, we analyzed between 400–600 contacts from four to six cells from one out of three similar experiments. To follow the integrin densities in Y-27632–treated cells (see Fig. 6), the average peak fluorescence intensities of 40–60 peripheral focal adhesions were measured.

FRAP

Control or dominant active Rac1/Ds red–transfected B16 β3–GFP cells were plated and grown on serum-coated glass coverslips in DMM/10%FCS for 24 h. For photo-bleaching and fluorescence recovery, the culture medium was changed to F12/10%FCS medium and cells were mounted on an inverted confocal microscope equipped with an incubation chamber (LSM510; Zeiss). Confocal images of focal adhesion sites were recorded with 2–3% of the intensity of the 488-nm line from living Mock and Rac1/Ds red–transfected cells. GFP fluorescence was eliminated using five bleach cycles at 100% intensity of the 488 line. Control bleach experiments performed over the entire cell surface demonstrated that the GFP chromophore was completely inactivated by this treatment and that recovery of fluorescence due to newly synthesized GFP proteins was not detectable during the period of recovery (15–20 min). Qualitative recovery curves (R[t]) were obtained per cell, by comparing fluorescence intensities of three to five bleached contacts (I$_{bleached\ contact}$[t]) with neighboring unbleached (I$_{unbleached\ contacts}$[t]) contacts after background (I$_{background}$[t]) subtraction: R(t) = (I$_{bleached\ contact}$[t] $-$ I$_{background}$[t])/(I$_{unbleached\ contacts}$[t] $-$ I$_{background}$[t]); t, time of recovery (White and Stelzer, 1999). This internal calibration compensated for intrinsic changes in fluorescence due to small focus changes and or the gradual loss of cellular GFP fluorescence during the observation period due to fluorophore inactivation by the laser. For comparison of several recovery curves, the fractional recovery (R$_{frac}$[t]) of each curve was

plotted against time. The analysis of the fractional recovery corrected for differences between cells due to incomplete inactivation of the chromophores during bleaching. Typically, the fluorescence intensity just after bleaching (I_{bleach}) was between 5 and 20% of the prebleach fluorescence (100%). The fractional recovery ($R_{frac}[t]$) (all curves start at 0) was therefore $R_{frac}(t) = (R[t] - I_{bleach})/(1 - I_{bleach})$ (Axelrod et al., 1976). A single logarithmic regression curve was calculated from the datapoints (Excel; Microsoft), in order to determine the half-maximal recovery time ($T_{1/2}$) and the MF ($MF = R_{frac}[t_{end}]$); t_{end} corresponds to the endpoint of the recovery period (10–15 min). Due to the variable size of the focal contacts analyzed, and a likely second order logarithmic recovery of integrins in focal contacts, a diffusion coefficient was not calculated. In addition, we did not correct the error that is due to the integrin fluorescence of the contact-overlaying membrane sheet in which the recovery is much faster (unpublished data). This error is more important for low- than high-density contacts, as the differences in the fluorescence between the membrane and high-density contacts is bigger than that for low-density contacts.

Online supplemental material

Video sequences of untreated and Rho-kinase inhibitor–treated β3–GFP-integrin–transfected cells reveal the dynamics of β3–GFP-containing adhesion sites. In addition, video sequences of cells cultured on elastic silicon substrata reveal the change in intracellular tension caused by the application of drugs. Video 1 demonstrates the stationary and transient nature of focal complexes appearing within an advancing lamellipodium. Video 2 reveals the apparent sliding of focal contacts localized within the rear of a migrating cell. Video 3 illustrates lamellipodia extension, collapse, and retraction in a nonmigratory cell, and follows the cycling of integrin fluorescence intensity as well as mobility between small and large focal adhesions. Video 4 demonstrates the increase in intracellular tension manifested by an increase in wrinkling of the flexible silicon substrate after LPA addition. Videos 5 and 6 illustrate the respective loss of intracellular tension after addition of Rho-kinase inhibitor (Y 27632 or staurosporine, respectively). Video 7 shows the behavioral and structural changes of β3–GFP–containing focal adhesion sites upon release of intracellular tension after inhibition of Rho-kinase. All videos are available at http://www.jcb.org/cgi/content/full/jcb.200107107/DC1.

References

Albelda, S.M., S.A. Mette, D.E. Elder, R. Stewart, L. Damjanovich, M. Herlyn, and C.A. Buck. 1990. Integrin distribution in malignant melanoma: association of the beta 3 subunit with tumor progression. *Cancer Res.* 50:6757–6764.

Amano, M., K. Chihara, K. Kimura, Y. Fukata, N. Nakamura, Y. Matsuura, and K. Kaibuchi. 1997. Formation of actin stress fibers and focal adhesions enhanced by Rho-kinase. *Science.* 275:1308–1311.

Anderson, K.I., and R. Cross. 2000. Contact dynamics during keratocyte motility. *Curr. Biol.* 10:253–260.

Axelrod, D., D.E. Koppel, J. Schlessinger, E. Elson, and W.W. Webb. 1976. Mobility measurement by analysis of fluorescence photobleaching recovery kinetics. *Biophys. J.* 16:1055–1069.

Balaban, N.Q., U.S. Schwarz, D. Riveline, P. Goichberg, G. Tzur, I. Sabanay, D. Mahalu, S. Safran, A. Bershadsky, L. Addadi, and B. Geiger. 2001. Force and focal adhesion assembly: a close relationship studied using elastic micropatterned substrates. *Nat. Cell Biol.* 3:466–472.

Ballestrem, C., B. Wehrle-Haller, and B.A. Imhof. 1998. Actin dynamics in living mammalian cells. *J. Cell Sci.* 111:1649–1658.

Ballestrem, C., B. Wehrle-Haller, B. Hinz, and B.A. Imhof. 2000. Actin-depen-

dent lamellipodia formation and microtubule-dependent tail retraction control-directed cell migration. *Mol. Biol. Cell.* 11:2999–3012.

Beningo, K.A., M. Dembo, I. Kaverina, J.V. Small, and Y.L. Wang. 2001. Nascent focal adhesions are responsible for the generation of strong propulsive forces in migrating fibroblasts. *J. Cell Biol.* 153:881–888.

Brooks, P.C., R.A. Clark, and D.A. Cheresh. 1994. Requirement of vascular integrin alpha v beta 3 for angiogenesis. *Science.* 264:569–571.

Chen, W.T. 1981. Mechanism of retraction of the trailing edge during fibroblast movement. *J. Cell Biol.* 90:187–200.

Cheresh, D.A., and R.C. Spiro. 1987. Biosynthetic and functional properties of an Arg-Gly-Asp-directed receptor involved in human melanoma cell attachment to vitronectin, fibrinogen, and von Willebrand factor. *J. Biol. Chem.* 262:17703–17711.

Chrzanowska-Wodnicka, M., and K. Burridge. 1996. Rho-stimulated contractility drives the formation of stress fibers and focal adhesions. *J. Cell Biol.* 133: 1403–1415.

Delannet, M., F. Martin, B. Bossy, D.A. Cheresh, L.F. Reichardt, and J.L. Duband. 1994. Specific roles of the alpha V beta 1, alpha V beta 3 and alpha V beta 5 integrins in avian neural crest cell adhesion and migration on vitronectin. *Development.* 120:2687–2702.

Dembo, M., and Y.L. Wang. 1999. Stresses at the cell-to-substrate interface during locomotion of fibroblasts. *Biophys. J.* 76:2307–2316.

Duband, J.L., G.H. Nuckolls, A. Ishihara, T. Hasegawa, K.M. Yamada, J.P. Thiery, and K. Jacobson. 1988. Fibronectin receptor exhibits high lateral mobility in embryonic locomoting cells but is immobile in focal contacts and fibrillar streaks in stationary cells. *J. Cell Biol.* 107:1385–1396.

Evans, G.I., G.K. Lewis, G. Ramsey, and M.J. Bishop. 1985. Isolation of monoclonal antibodies specific for human c-myc proto-oncogene product. *Mol. Cell Biol.* 5:3610–3616.

Felding-Habermann, B., T.E. O'Toole, J.W. Smith, E. Fransvea, Z.M. Ruggeri, M.H. Ginsberg, P.E. Hughes, N. Pampori, S.J. Shattil, A. Saven, and B.M. Mueller. 2001. Integrin activation controls metastasis in human breast cancer. *Proc. Natl. Acad. Sci. USA.* 98:1853–1858.

Fincham, V.J., M. James, M.C. Frame, and S.J. Winder. 2000. Active ERK/MAP kinase is targeted to newly forming cell-matrix adhesions by integrin engagement and v-Src. *EMBO J.* 19:2911–2923.

Geiger, B., and A. Bershadsky. 2001. Assembly and mechanosensory function of focal contacts. *Curr. Opin. Cell Biol.* 13:584–592.

Harris, A.K., P. Wild, and D. Stopak. 1980. Silicone rubber substrata: a new wrinkle in the study of cell locomotion. *Science.* 208:177–179.

Heino, J., R.A. Ignotz, M.E. Hemler, C. Crouse, and J. Massague. 1989. Regulation of cell adhesion receptors by transforming growth factor-beta. Concomitant regulation of integrins that share a common beta 1 subunit. *J. Biol. Chem.* 264:380–388.

Horwitz, A.R., and J.T. Parsons. 1999. Cell migration—movin' on. *Science.* 286: 1102–1103.

Hughes, P.E., M.W. Renshaw, M. Pfaff, J. Forsyth, V.M. Keivens, M.A. Schwartz, and M.H. Ginsberg. 1997. Suppression of integrin activation: a novel function of a Ras/Raf-initiated MAP kinase pathway. *Cell.* 88:521–530.

Hynes, R.O. 1992. Integrins: versatility, modulation, and signaling in cell adhesion. *Cell.* 69:11–25.

Iwanaga, Y., D. Braun, and P. Fromherz. 2001. No correlation of focal contacts and close adhesion by comparing GFP-vinculin and fluorescence interference of DiI. *Eur. Biophys. J.* 30:17–26.

Jalali, S., M.A. del Pozo, K. Chen, H. Miao, Y. Li, M.A. Schwartz, J.Y. Shyy, and S. Chien. 2001. Integrin-mediated mechanotransduction requires its dynamic interaction with specific extracellular matrix (ECM) ligands. *Proc. Natl. Acad. Sci. USA.* 98:1042–1046.

Katz, B.Z., E. Zamir, A. Bershadsky, Z. Kam, K.M. Yamada, and B. Geiger. 2000. Physical state of the extracellular matrix regulates the structure and molecular composition of cell-matrix adhesions. *Mol. Biol. Cell.* 11:1047–1060.

Kimura, K., M. Ito, M. Amano, K. Chihara, Y. Fukata, M. Nakafuku, B. Yamamori, J. Feng, T. Nakano, T. Okawa, et al. 1996. Regulation of myosin phosphatase by Rho and Rho-associated kinase (Rho-kinase). *Science.* 273:245–248.

Kiosses, W.B., S.J. Shattil, N. Pampori, and M.A. Schwartz. 2001. Rac recruits high-affinity integrin alphavbeta3 to lamellipodia in endothelial cell migration. *Nat. Cell. Biol.* 3:316–320.

Klemke, R.L., S. Cai, A.L. Giannini, P.J. Gallagher, P. de Lanerolle, and D.A. Cheresh. 1997. Regulation of cell motility by mitogen-activated protein kinase. *J. Cell Biol.* 137:481–492.

LaFlamme, S.E., L.A. Thomas, S.S. Yamada, and K.M. Yamada. 1994. Single subunit chimeric integrins as mimics and inhibitors of endogenous integrin

functions in receptor localization, cell spreading and migration, and matrix assembly. *J. Cell Biol.* 126:1287–1298.

Lauffenburger, D.A., and A.F. Horwitz. 1996. Cell migration: a physically integrated molecular process. *Cell.* 84:359–369.

Lee, J., and K. Jacobson. 1997. The composition and dynamics of cell-substratum adhesions in locomoting fish keratocytes. *J. Cell Sci.* 110:2833–2844.

Legler, D.F., G. Wiedle, F.P. Ross, and B.A. Imhof. 2001. Superactivation of integrin alphavbeta3 by low antagonist concentrations. *J. Cell Sci.* 114:1545–1553.

Lenter, M., and D. Vestweber. 1994. The integrin chains beta 1 and alpha 6 associate with the chaperone calnexin prior to integrin assembly. *J. Biol. Chem.* 269:12263–12268.

Lo, C.M., H.B. Wang, M. Dembo, and Y.L. Wang. 2000. Cell movement is guided by the rigidity of the substrate. *Biophys. J.* 79:144–152.

Machesky, L.M., and A. Hall. 1997. Role of actin polymerization and adhesion to extracellular matrix in Rac- and Rho-induced cytoskeletal reorganization. *J. Cell Biol.* 138:913–926.

McHugh, K.P., K. Hodivala-Dilke, M.H. Zheng, N. Namba, J. Lam, D. Novack, X. Feng, F.P. Ross, R.O. Hynes, and S.L. Teitelbaum. 2000. Mice lacking beta3 integrins are osteosclerotic because of dysfunctional osteoclasts. *J. Clin. Invest.* 105:433–440.

Miyamoto, S., H. Teramoto, O.A. Coso, J.S. Gutkind, P.D. Burbelo, S.K. Akiyama, and K.M. Yamada. 1995. Integrin function: molecular hierarchies of cytoskeletal and signaling molecules. *J. Cell Biol.* 131:791–805.

Niggli, V. 1999. Rho-kinase in human neutrophils: a role in signalling for myosin light chain phosphorylation and cell migration. *FEBS Lett.* 445:69–72.

Nobes, C.D., and A. Hall. 1995. Rho, rac, and cdc42 GTPases regulate the assembly of multimolecular focal complexes associated with actin stress fibers, lamellipodia, and filopodia. *Cell.* 81:53–62.

Nobes, C.D., and A. Hall. 1999. Rho GTPases control polarity, protrusion, and adhesion during cell movement. *J. Cell Biol.* 144:1235–1244.

Oliver, T., M. Dembo, and K. Jacobson. 1999. Separation of propulsive and adhesive traction stresses in locomoting keratocytes. *J. Cell Biol.* 145:589–604.

Palecek, S.P., A. Huttenlocher, A.F. Horwitz, and D.A. Lauffenburger. 1998. Physical and biochemical regulation of integrin release during rear detachment of migrating cells. *J. Cell Sci.* 111:929–940.

Pankov, R., E. Cukierman, B.Z. Katz, K. Matsumoto, D.C. Lin, S. Lin, C. Hahn, and K.M. Yamada. 2000. Integrin dynamics and matrix assembly: tensin-dependent translocation of alpha(5)beta(1) integrins promotes early fibronectin fibrillogenesis. *J. Cell Biol.* 148:1075–1090.

Pelham, R.J., Jr., and Y. Wang. 1997. Cell locomotion and focal adhesions are regulated by substrate flexibility. *Proc. Natl. Acad. Sci. USA.* 94:13661–13665.

Pierini, L.M., M.A. Lawson, R.J. Eddy, B. Hendey, and F.R. Maxfield. 2000. Oriented endocytic recycling of alpha5beta1 in motile neutrophils. *Blood.* 95:2471–2480.

Plancon, S., M.C. Morel-Kopp, E. Schaffner-Reckinger, P. Chen, and N. Kieffer. 2001. Green fluorescent protein (GFP) tagged to the cytoplasmic tail of alphaIIb or beta3 allows the expression of a fully functional integrin alphaIIb(beta3): effect of beta3GFP on alphaIIb(beta3) ligand binding. *Biochem. J.* 357:529–536.

Ridley, A.J., and A. Hall. 1992. The small GTP-binding protein rho regulates the assembly of focal adhesions and actin stress fibers in response to growth factors. *Cell.* 70:389–399.

Ridley, A.J., H.F. Paterson, C.L. Johnston, D. Diekmann, and A. Hall. 1992. The small GTP-binding protein rac regulates growth factor-induced membrane ruffling. *Cell.* 70:401–410.

Rivas, G., K. Tangemann, A.P. Minton, and J. Engel. 1996. Binding of fibrinogen to platelet integrin alpha IIb beta 3 in solution as monitored by tracer sedimentation equilibrium. *J. Mol. Recognit.* 9:31–38.

Riveline, D., E. Zamir, N.Q. Balaban, U.S. Schwarz, T. Ishizaki, S. Narumiya, Z. Kam, B. Geiger, and A.D. Bershadsky. 2001. Focal contacts as mechanosensors: externally applied local mechanical force induces growth of focal contacts by an mDia1-dependent and ROCK-independent mechanism. *J. Cell Biol.* 153:1175-86.

Rottner, K., A. Hall, and J.V. Small. 1999. Interplay between Rac and Rho in the control of substrate contact dynamics. *Curr. Biol.* 9:640–648.

Ruiz, P., D. Dunon, A. Sonnenberg, and B.A. Imhof. 1993. Suppression of mouse melanoma metastasis by EA-1, a monoclonal antibody specific for alpha 6 integrins. *Cell. Adhes. Commun.* 1:67–81 (published erratum appears in *Cell. Adhes. Commun.* 1993. 2:190).

Sanders, L.C., F. Matsumura, G.M. Bokoch, and P. de Lanerolle. 1999. Inhibition of myosin light chain kinase by p21-activated kinase. *Science.* 283:2083–2085.

Smilenov, L.B., A. Mikhailov, R.J. Pelham, E.E. Marcantonio, and G.G. Gundersen. 1999. Focal adhesion motility revealed in stationary fibroblasts. *Science.* 286:1172–1174.

Svitkina, T.M., A.B. Verkhovsky, K.M. McQuade, and G.G. Borisy. 1997. Analysis of the actin-myosin II system in fish epidermal keratocytes: mechanism of cell body translocation. *J. Cell Biol.* 139:397–415.

Takahashi, K., T. Nakamura, M. Koyanagi, K. Kato, Y. Hashimoto, H. Yagita, and K. Okumura. 1990. A murine very late activation antigen-like extracellular matrix receptor involved in CD2- and lymphocyte function-associated antigen-1-independent killer-target cell interaction. *J. Immunol.* 145:4371–4379.

Uehata, M., T. Ishizaki, H. Satoh, T. Ono, T. Kawahara, T. Morishita, H. Tamakawa, K. Yamagami, J. Inui, M. Maekawa, and S. Narumiya. 1997. Calcium sensitization of smooth muscle mediated by a Rho-associated protein kinase in hypertension. *Nature.* 389:990–994.

van Leeuwen, F.N., S. van Delft, H.E. Kain, R.A. van der Kammen, and J.G. Collard. 1999. Rac regulates phosphorylation of the myosin-II heavy chain, actinomyosin disassembly and cell spreading. *Nat. Cell Biol.* 1:242–248.

Weerasinghe, D., K.P. McHugh, F.P. Ross, E.J. Brown, R.H. Gisler, and B.A. Imhof. 1998. A role for the alphavbeta3 integrin in the transmigration of monocytes. *J. Cell Biol.* 142:595–607.

White, J., and E. Stelzer. 1999. Photobleaching GFP reveals protein dynamics inside live cells. *Trends Cell Biol.* 9:61–65.

Worthylake, R.A., S. Lemoine, J.M. Watson, and K. Burridge. 2001. RhoA is required for monocyte tail retraction during transendothelial migration. *J. Cell Biol.* 154:147–160.

Yauch, R.L., D.P. Felsenfeld, S.K. Kraeft, L.B. Chen, M.P. Sheetz, and M.E. Hemler. 1997. Mutational evidence for control of cell adhesion through integrin diffusion/clustering, independent of ligand binding. *J. Exp. Med.* 186:1347–1355.

Zamir, E., M. Katz, Y. Posen, N. Erez, K.M. Yamada, B.Z. Katz, S. Lin, D.C. Lin, A. Bershadsky, Z. Kam, and B. Geiger. 2000. Dynamics and segregation of cell-matrix adhesions in cultured fibroblasts. *Nat. Cell. Biol.* 2:191–196.